RSC Advances

PAPER

View Article Online
View Journal | View Issue

Cite this: *RSC Adv.*, 2020, **10**, 11348

Effect of surface interactions on the settlement of particles on a sinusoidally corrugated substrate†

Shreya Erramilli,[a] Taylor V. Neumann,[b] Daniel Chester,[cd] Michael D. Dickey,[b] Ashley C. Brown[cd] and Jan Genzer[*b]

Received 8th December 2019
Accepted 6th March 2020

DOI: 10.1039/c9ra10297c

rsc.li/rsc-advances

Naturally-occurring surface topographies abound in nature and endow diverse properties, *i.e.*, superhydrophobicity, adhesion, anti-fouling, self-cleaning, anti-glare, anti-bacterial, and many others. Researchers have attempted to replicate such topographies to create human-made surfaces with desired functionalities. For example, combining the surface topography with judicial chemical composition could provide an effective, non-toxic solution to combat non-specific biofouling. A systematic look at the effect of geometry, modulus, and chemistry on adhesion is warranted. In this work, we use a model system that comprises silica (SiO_x) beads interacting with a substrate made of a commercial polydimethylsiloxane kit (PDMS, Sylgard 184) featuring a sinusoidal topography. To examine the impact of interactions on particle settlement, we functionalize the surfaces of both the PDMS substrate and the SiO_x beads with polyacrylic acid (PAA) and polyethyleneimine (PEI), respectively. We also use the PDMS commercial kit coated with liquid glass (LG) to study the effect of the substrate modulus on particle settlement. Substrates with a higher aspect ratio (*i.e.*, amplitude/periodicity) encourage adsorption of particles along the sides of the channel compared with substrates with lower aspect ratio. We employ colloidal probe microscopy to demonstrate the effect of interaction between the substrate and the particle. The interplay among the surface modulus, geometry, and interactions between the surface and the particle governs particle settlement on sinusoidally-corrugated substrates.

Introduction

Understanding the interactions between surfaces and their environment is crucial to the performance of paints, waterproof clothing, non-stick cookware, adhesives, anti-glare lenses, and other aspects of daily life. The performance characteristics of substrates can be traced to the geometry, chemical composition, and mechanical properties of the surface. Topographical patterns on a surface can contain long-range or short-range order features and can exhibit functionalities such as superhydrophobicity,[1] anti-fouling properties,[2] reversible adhesion,[3] and wettability characteristics.[4,5] Aspects of surfaces such as the topographical pattern, chemistry, and modulus can lead to an increased surface area and anisotropy, and may be employed in many applications.[6]

Understanding non-specific biological fouling is pertinent to improving the performance of membranes, biomedical devices, and shipping vessels, among others.[5–11] In the context of the marine environment, fouling caused by barnacle attachment on ship hulls increases drag and results in higher fuel consumption[12] as well as ecological disruption when species are transported by ships over long distances.[13] To inhibit adhesion of marine organisms, hulls of ships have traditionally been coated with biocidal organometallic compounds, such as tributyltin. Unfortunately, leaching of these compounds into the ocean results in adverse consequences for marine life, which led to its widespread ban.[14] Alternate strategies to combat fouling in various applications are based on using antifouling and foul-release chemistries.[15] Increasingly, the focus has been on creating non-toxic antifouling coatings by taking advantage of surface topographical features[16–22] inspired by examples found in nature.[23–26]

Although the use of nature-inspired surface topography to mitigate biofouling is an ongoing area of research, the problem is complex due to the vast array of different shapes and sizes as well as chemistries taken by fouling organisms.[27] Fouling species vary in size from nm (*i.e.*, proteins) to cm (*i.e.*, barnacles or tubeworms).[28] This diversity presents a challenge to designing a topography-based antifouling surface because the topographical features needed to prevent biofouling depend

[a]*Department of Materials Science & Engineering, North Carolina State University, Raleigh, NC 27695-7907, USA*

[b]*Department of Chemical & Biomolecular Engineering, North Carolina State University, Raleigh, NC 27695-7905, USA. E-mail: jgenzer@ncsu.edu*

[c]*Joint Department of Biomedical Engineering, North Carolina State University, University of North Carolina at Chapel Hill, Raleigh, NC 27695-7115, USA*

[d]*Comparative Medicine Institute, North Carolina State University, Raleigh, NC 27695-7905, USA*

† Electronic supplementary information (ESI) available. See DOI: 10.1039/c9ra10297c

upon the size and shape of settling organisms. Designing a surface that prevents the settlement of organisms over a broad size range requires further study.[29] Numerous researchers created bioinspired surfaces to generate anti-fouling surfaces. Lotus leaves, shark skin, and the carapace of crabs have all been replicated to attempt to develop a suitable surface to prevent settlement of marine organisms.[30–33] Researchers have applied attachment point theory to explain the effect of surface topography on preventing settlement. De Nys *et al.*[34,35] state that relative sizes of settling organisms and surface topography affect the number of attachment points between the surface and organism, which contributes to the anti-fouling behavior of the surface.

Formation and behavior of wrinkles on surfaces and their effect on behavior of particles on the surface have been studied previously.[36] Hierarchical wrinkles, *i.e.*, concurrent wrinkles over multiple length scales have been created by exposing stretched PDMS to ultraviolet (UV) light and releasing the strain and have been used to fractionate particles based on size.[37] Surface topography generated by wrinkles has also been used to enable assembly of particles into desired conformations.[38] Research by the Fery group has shown that wrinkled surfaces can direct the arrangement of colloidal particles of varying size, surface chemistry, and shape.[39] However, reliance on wrinkled surfaces limits the aspect ratios, which can be generated. In-silica studies have no such limitations. Schoch *et al.*[40–42] employed Monte Carlo simulation schemes to model the settlement of spherical particles on model sinusoidal substrates of an array of aspect ratios. The results revealed that particle settlement was minimal when the particle diameter was half the substrate wavelength. The addition of polymeric 'hairs' on the surface of the particles increased the likelihood of settlement on the surface regardless of substrate geometry because they resulted in increased interaction between the particles and substrate.

In this work, we consider a model experimental system comprising spherical particles and a substrate featuring sinusoidal topography (*cf.* Fig. 1). We control the interactions between the settling particle and the substrate features by varying the size of the substrate features and the particle (*cf.* Fig. 1a), the chemistry of the substrate, and the particle (*cf.* Fig. 1b), and the substrate modulus. We monitor the effect of the parameters mentioned earlier on the location of particles settled on the substrate, which we assess by using optical microscopy (*cf.* Fig. 1c) and laser scanning confocal microscopy (*cf.* Fig. 1d). By visualizing the settlement of particles on sinusoidal surfaces using 3D imaging techniques (both appropriately modified), we can quantify the effect of changing surface geometry as well as surface chemistry on the settlement of particles. We further employ colloidal force microscopy (CFM) to quantify the interactions between the surface and the particle as a function of changing the surface chemistry and the modulus. In the sections that follow, we will describe how we fabricate the substrate and achieve the settlement of particles. We also describe the modification of a CFM tip with a spherical particle to probe the surface and measure the interactions between surface and particle.

Materials and experimental methods

We 3D printed a series of master molds featuring a sinusoidal surface topography (see ESI† for details). Replicas of each master mold were fabricated using Sylgard 184 poly(-dimethylsiloxane) kit (hereafter referred to as PDMS) using a 10 : 1 base to curing agent ratio followed by an overnight cure at 50 °C. All subsequent experiments were performed on the PDMS replicas. The geometric parameters of the PDMS substrates are defined by the wavelength (λ) and amplitude (A), as shown in Fig. 2, and the aspect ratio (AR = A/λ). The 3D printed substrates feature AR values of 0.69, 1.0, and 1.13. To alter the interactions between the substrate and the particles, we activated the PDMS substrate with ultraviolet/ozone (UVO) treatment and used layer-by-layer (LbL) deposition of poly (ethylene amine) (PEI) and poly(acrylic acid) (PAA). We first exposed the corrugated PDMS replicas to UVO for 20 minutes. The PEI solution was 20 mg mL^{-1} in ethanol, and the PAA solution was 16 mg mL^{-1} in deionized (DI) water, and the pH is adjusted from 2.9 to 4.3 using sodium hydroxide (NaOH). We then immersed the UVO-modified PDMS substrates in the PEI solution for 2 minutes, and after removal from the solution, we annealed the specimens at 70 °C in air. Subsequently, we immersed the substrates in the PAA solution for 2 minutes, removed them from the deposition solution, and annealed them at 70 °C. Fig. 1b displays pictorially the system set up. Previous literature reports show that the thickness of PEI and PAA layers was approximately 2–3 nm.[43]

We deposited liquid glass (LG) on the PDMS surface to increase the local surface modulus of the substrate to examine its effect on the settlement of the particles. We first UVO treated the PDMS surface for 20 minutes, followed by PEI treatment, as

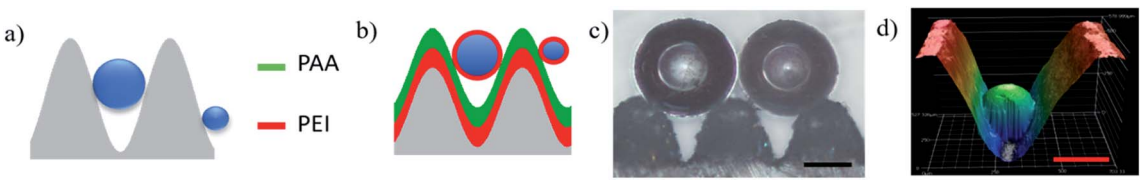

Fig. 1 The position of a settling spherical particle depends on interactions with the surface. Cartoons in (a) and (b) show the effect of substrate geometry and interactions between the surface and the particle on the location of the particle. (c) Optical microscopy image of spherical SiO_x particle settling upon sinusoidal PDMS channels. Scale bar: 200 μm. (d) Laser scanning microscopy image of a particle settling in between sinusoidal features. The colors represent different depths inside the specimen. Scale bar: 500 μm.

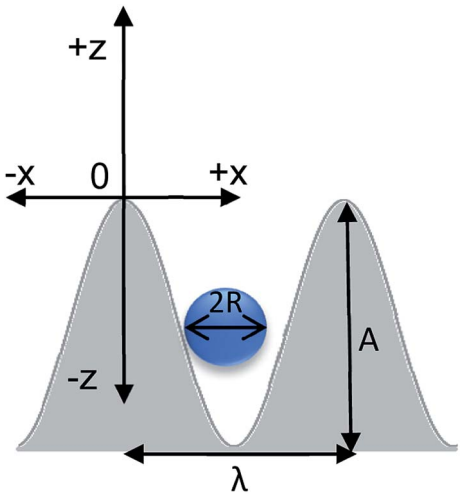

Fig. 2 Dimensions of the substrate–particle system. Parameters to consider are amplitude (A), wavelength (λ), particle radius (R). The coordinate system used in the analysis is also depicted.

described earlier. We washed away the excess of PEI with ethanol before drying the specimens for 30 minutes at 70 °C. Drops of a solution comprising LG 3.7 weight% in DI water were added to the surface, and the system was cured overnight at 70 °C. Subsequently, the PDMS substrate was UVO treated for another 20 minutes before we applied the deposition sequence of PEI and PAA layers to functionalize the LG surface. We deposited polydisperse silica (SiO_x) particles having the radii of 100–150 μm and 200–250 μm on the substrates (*vide infra*). We modified the surface of the SiO_x beads as follows. We cleaned the SiO_x beads using a piranha solution and rinsed thoroughly with DI water and ethanol. We then immersed these SiO_x beads in the PEI solution in ethanol for 15 minutes, rinsed with pure ethanol, and annealed at 70 °C overnight.

We affixed each substrate to a stage and immersed it into a vessel containing a mixture of particles in water. We agitated the particle/water mixture using compressed air, and the particles settled upon the surfaces by gravity. The substrates were removed from the solution and were dried at ambient conditions. We used an Olympus BX60 optical microscope using the 5× and 20× objectives, as well as the Keyence laser scanning confocal microscope using the 20× objective to image the particle–substrate system.

We employed colloidal probe microscopy (CPM) to study the effect surface chemistry on interactions between the SiO_x particle and the substrate. CPM probes with pyramidal tips were acquired from Asylum Research and were modified such that an unmodified, or PEI-coated SiO_x particle was attached to the cantilever with a thermoplastic wax adhesive.[44] These modified tips were used to probe flat PDMS and PDMS:UVO/LG substrates, which were chemically modified using the processes described above. We employed an Asylum Research MFP-3D AFM instrument to obtain a force map. The surface stiffness of each sample was measured using the spherical tip geometry, and the Hertz model of adhesion. We determined the work done to separate the particle from the substrate by measuring the area between the approach and retraction curves in the CPM.

Results and discussion

We monitored the location of SiO_x particles on the corrugated PDMS substrates as a function of the surface aspect ratio of the substrate and chemical modification of the substrate and the particles. The PDMS surface features a sinusoidal topography, and the SiO_x particle is a sphere with a radius R. As depicted in Fig. 2, the origin of the coordinate system is located at the top of the sinusoidal curve. Only one half of the wavelength is considered due to the symmetry of the system. The curve is described as a function of x (in-plane coordinate) and z (depth coordinate). In this 2D projection, the sphere reduces to a circle of the same radius. The center of the sphere (COS) is given by the coordinates $[x', z']$. We obtain the x' and z' coordinates from images collected by the laser scanning microscopy. Details about the methodology used to calculate the COS are provided in ESI.†

In Fig. 3 and 5, we plot the position of the center of the SiO_x particle normalized by the substrate periodicity (λ). We plot $(z' - R/A)$ *versus* z'/λ to compare data collected from substrates featuring multiple AR. The coordinates of the COS of a particle that rests on top of the sinusoidal feature appears at the origin are [0, 0]. Particles small enough to settle in the bottom of the channel the position will have the COS coordinates [0.5, −1]. The black and blue lines in Fig. 3 and 5 serve as a visual guide for the expected location of particles having a diameter of 100 and 200 μm on each substrate, respectively. Fig. S6 in ESI† and the accompanying discussion describe how these lines have been calculated. The symbols depict experimental data. Table 1 lists the attributes systems we explored in this study.

The data in Fig. 3 describe the settlement of the SiO_x particles as a function of changing the AR of the PDMS substrate features. In Fig. 3a, nearly all particles settle preferentially on the bottom of the channel (AR = 0.69). Increasing the AR to 1 (Fig. 3b) causes the larger particles to settle in the valley of the substrate while the smaller particles show more dispersion along the sides of the channel. For substrates with AR = 0.69 and AR = 1, modification of the particle surface with PEI causes the smaller particles to settle along the sides of the channel. The same is true when both the substrate and the particles are chemically modified. Upon increasing the AR to 1.13 (Fig. 3c) particles exhibit increased dispersion along the sides of the channel regardless of the substrate and particle surface modification. Thus, as the AR increases, the deviation of particles away from the center increases. This means that more particles settle along the sides of the sinusoidal features. Particles of smaller diameter appear to be more sensitive to this effect more than larger particles, and surface modification of substrate and particle appears to facilitate this behavior.

We now consider the effect of the substrate modulus on particle settlement. If particles settle along the sides of the sinusoidal channel while increasing the AR, they may get trapped in a metastable state at the surface due to a compliant substrate. We observed this phenomenon using optical

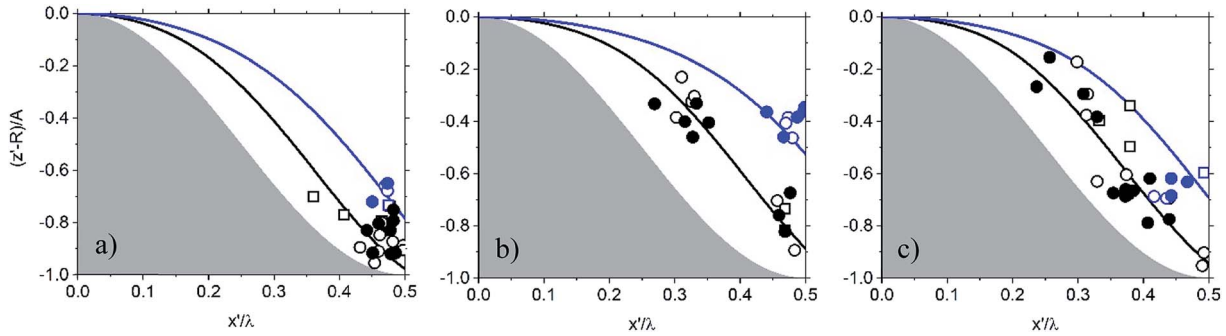

Fig. 3 Settlement of silica particles mapped on the PDMS substrate as a function of increasing aspect ratio, AR, (A/λ), where A and λ represent the feature amplitude and wavelength, respectively: (a) AR = 0.69, (b) AR = 1, (c) AR = 1.13. x' and z' describe particle center. The shaded area represents the substrate. Particle is mapped on axes normalized to λ and A. When (x', z') is (0, 0), the particle is at the top of the sinusoid and when it is (0.5, −1) the particle is at the bottom of the sinusoidal channel. Symbols represent different surface and particle interactions where squares indicate unmodified PDMS surface and particle surface. Circles indicate the surface of PDMS has been modified with PEI. Stars indicate that the PDMS surface has been modified with PEI, and particle surface has been modified with PAA. Refer to Table 1 for mapping symbol type to system surface chemistries. The black and blue symbols and lines correspond to the settlement of particles with nominal diameters of ~100 μm and ~200 μm, respectively.

microscopy (*cf.* Fig. 4). Here, we captured images of corrugated substrates with a square cross-sectional profile before and after the deposition of SiO_x particles. Fig. 4a shows the parallel features of the corrugations. After introducing the particles, we observed the deformation of the features caused by the SiO_x particles, as shown in Fig. 4b. A cross-sectional view shown in Fig. 4c shows the perpendicular sides of the valleys deforming in response to the particle settlement.

To observe the effect surface modulus on particle settlement, we coat the sinusoidally patterned PDMS substrates with a layer comprising LG and carry out the same chemical surface modification steps used in Fig. 3. Particle deposition and imaging are carried out as before, and the results are shown in Fig. 5, where AR increases from 0.69 (Fig. 5a) to 1 (Fig. 5a), and 1.13 (Fig. 5c). In Fig. 5a, the particles settle to the bottom of the channel. Upon increasing the AR to 1 (Fig. 5b), the SiO_x particles reside in either the center or close to the center of the channel. In Fig. 5c, we observe minimal dispersion along the sides of the channel. Particle settlement remains unchanged despite the increase in AR as well as altering interactions between the substrate and the particles. The dispersion of particles along the surface of the sinusoid appears to be independent of the surface functionalization of the SiO_x beads and the modulus of the PDMS surface.

Next, we quantified the effect of surface chemistry on the interactions between the substrate and the particles. We modified an AFM tip by attaching a particle to the end of it and used it to probe the interaction with various substrates. All substrates were flat. We attach an unmodified and PEI-modified SiO_x bead to the AFM tips. The substrates probed include PDMS and PDMS:UVO coated with LG. We functionalize both these substrates with PAA. Fig. 6–8 depict the approach and retraction curves of each of the above conditions in the CFM. The area between the approach and retraction curves represents the work done to separate the particle from the surface (*vide infra*). We measure the surface modulus in each case and plot the values in Fig. S10 and S11.† Average moduli are reported in Table S2.†

Fig. 6 demonstrates the use of the approach and retraction curves collected by CFM to measure interactions between the substrate and the particle without chemical modification. Fig. 6a reports the force corresponding to the approach (black) and retraction (red) of the tip modified with SiO_x particles as it interacts with the PDMS substrate. The low modulus of the substrate gives rise to a high contact area between the substrate

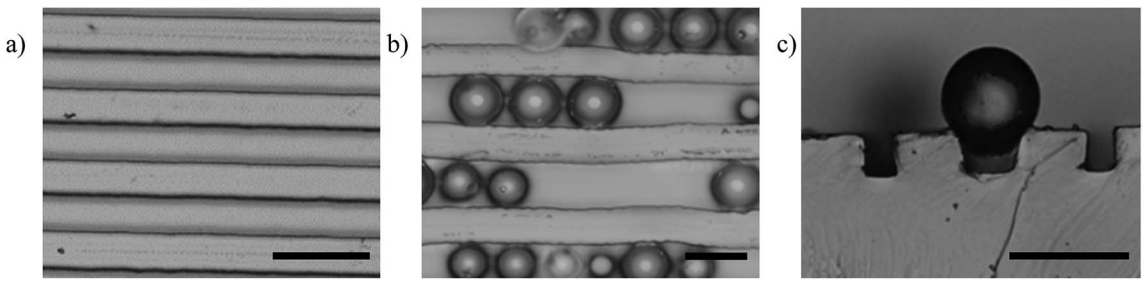

Fig. 4 The deformation of PDMS features by silica (SiO_x) particles is shown on corrugated surfaces with a square profile using optical microscopy in reflectance mode. (a) Surface before silica particle deposition shows parallel features. Scale bar: 200 μm. (b) Silica particles once deposited cause the features to deform around the particle. Scale bar: 50 μm. (c) A cross-sectional view of the substrate with particle shows perpendicular features deforming due to the particle. Scale bar: 50 μm.

Table 1 Parameters of systems studied in this work

Substrate	Particle	Symbols in Fig. 3 and 5
PDMS	SiO_x	Open squares (□)
PDMS-UVO/PAA	SiO_x	Open circles (○)
PDMS-UVO/PAA	SiO_x/PEI	Closed circles (●)
PDMS-UVO/PEI/LG	SiO_x	Open up-triangles (△)
PDMS-UVO/PEI/LG/PAA	SiO_x	Open down-triangles (▽)
PDMS-UVO/PEI/LG/PAA	SiO_x/PEI	Closed down-triangles (▼)

and particle. This is seen in the well of the retraction curve as well as the high area between the curves. Fig. 6b shows the approach and retraction curves for the LG-coated PDMS:UVO substrate as it is probed by the bare SiO_x particle. The higher surface modulus (due to UVO treatment of PDMS) reduces the area of contact between the substrate and the particle.[37] The lack of separation between the approach and retraction curves indicates that upon separation of the two surfaces, the interactions between the two surfaces are weak (see inset to Fig. 6b).

Fig. 7a plots the force between the PDMS:UVO surface modified with PAA and an unmodified SiO_x particle. Fig. 7b plots data corresponding to the LG-coated PDMS:UVO substrate modified with PAA indented with an AFM tip modified with a SiO_x sphere. Because the PDMS:UVO substrate has a lower modulus than the PDMS:UVO/LG one, the contact area between the particle and substrate is higher in the former case, and it gives rise to a large contact area between the substrate and the particle. Thus, more work needs to be done to separate the particle from the LG-free substrate. The increased modulus of

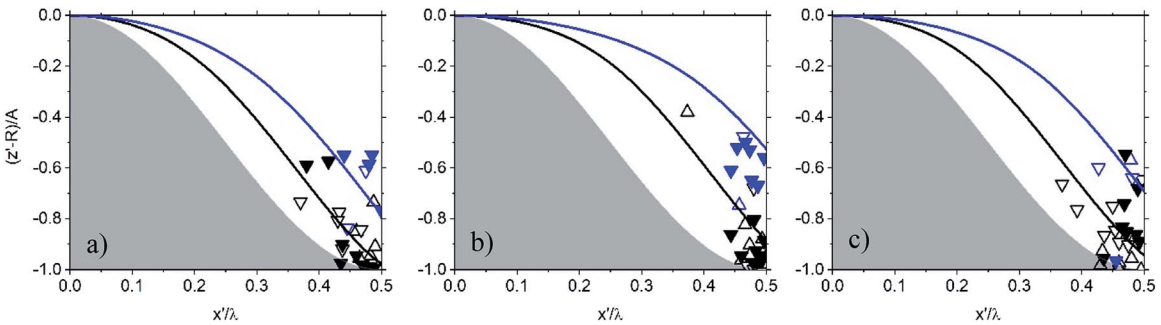

Fig. 5 The settlement of silica particles mapped on the PDMS:UVO substrate coated with LG as a function of increasing aspect ratio, AR, where A and λ represent the feature amplitude and wavelength, respectively: (a) AR = 0.69, (b) AR = 1, (c) AR = 1.13. x' and z' describe particle center. The shaded area represents the substrate. Particles are mapped on axes normalized to λ and A. When (x', z') is (0, 0), the particle is at the top of the sinusoid and when it is (0.5, −1) the particle is at the bottom of the sinusoidal channel. Symbols represent different surface and particle interactions where squares indicate unmodified PDMS/LG surface and particle surface. Circles indicate the surface of PDMS:UVO/LG has been modified with PEI. Stars indicate that PDMS:UVO/LG surface has been modified with PEI, and the particle surface has been modified with PAA. Refer to Table 1 for mapping symbol type to system surface chemistries. The black and blue symbols and lines correspond to the settlement of particles with nominal diameters of ~100 μm and ~200 μm, respectively.

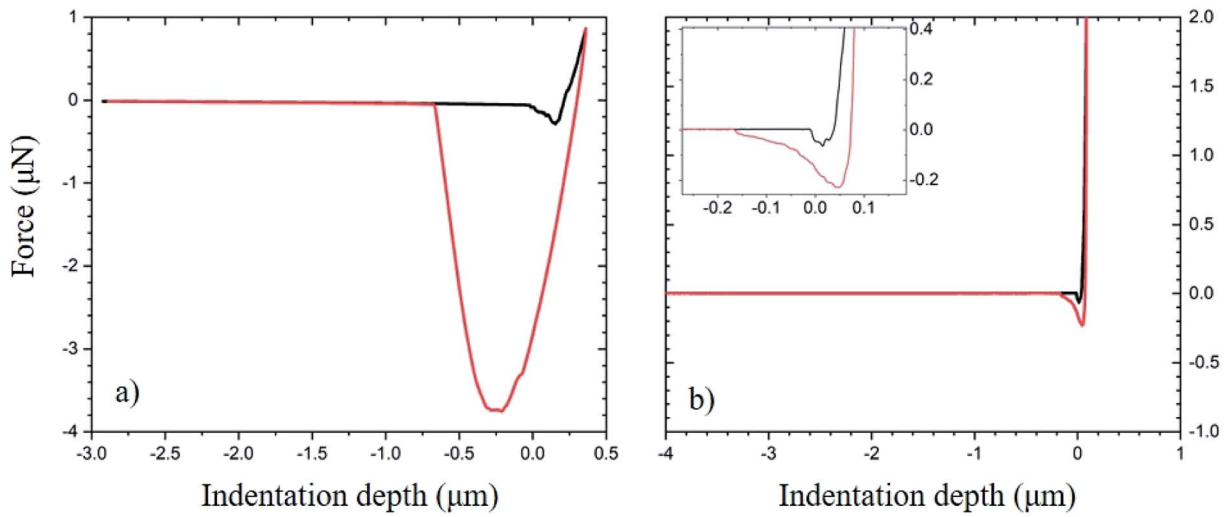

Fig. 6 Force resulting from interactions between unfunctionalized substrates and particles measured using AFM. (a) Approach (black data) and retrace (red data) when a spherical SiO_x particle is used to probe a PDMS surface. (b) Approach and retrace data for PDMS:UVO surface coated with LG and probed with a spherical SiO_x particle.

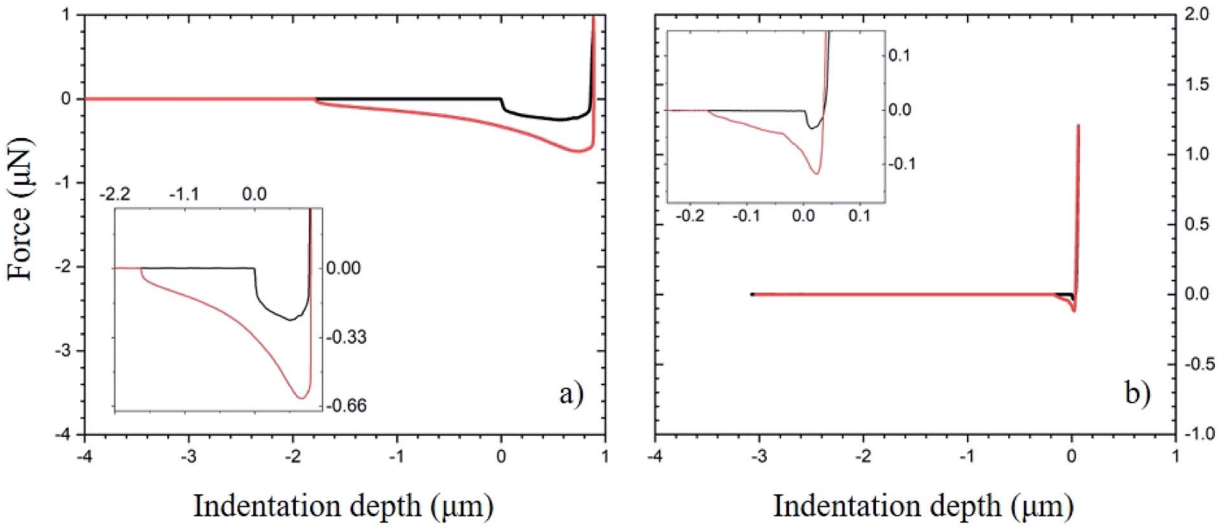

Fig. 7 Force resulting from interactions between PAA-functionalized substrates and unfunctionalized particles. (a) Approach (black data) and retrace (red data) when a spherical SiO_x particle is used to probe a PDMS surface modified with the PAA surface. (b) Approach and retrace data for PDMS surface coated with LG, functionalized with PAA probed with a spherical SiO_x particle.

the LG coating results in the decreased contact area between the particle and the substrate, thus resulting in weaker adhesion (see inset to Fig. 7b).

Fig. 8 displays data depicting the interaction in systems where both the substrate and the SiO_x particle surfaces have been functionalized by PAA and PEI, respectively. In Fig. 8a, we

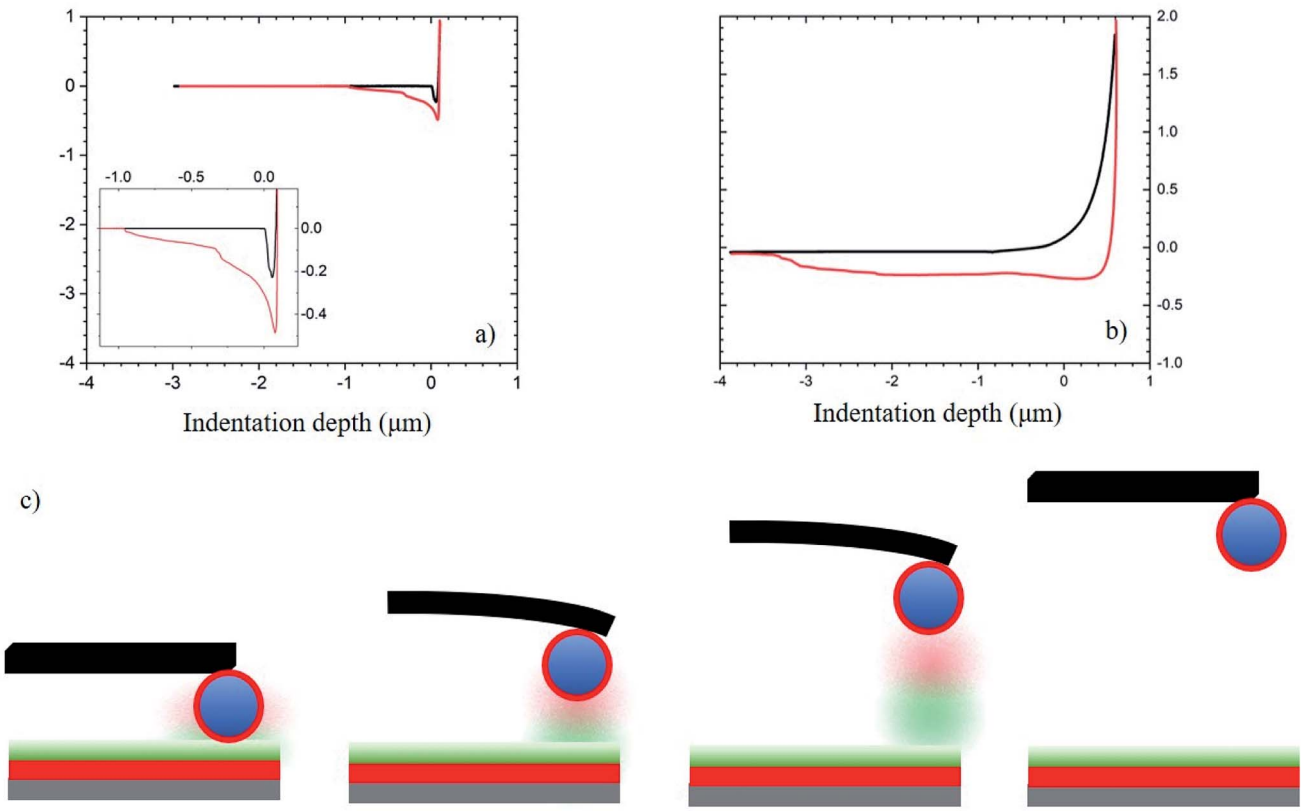

Fig. 8 AFM traces of interactions between PAA-functionalized substrates and PEI–SiO_x particles. (a) Approach (black data) and retrace (red data) when a particle probes a PDMS surface modified with PAA. (b) Approach and retrace data for PDMS coated with LG and functionalized with PAA. (c) The effect of functionalization on the interactions between the surfaces. Red represents PEI, and green represents PAA. Red and green clouds depict the interactions between the PAA and PEI layers.

plot the results corresponding to interactions between PDMS:UVO substrate modified with a PAA layer and a particle modified with PEI coating. The work needed to separate the particle from the surface is lower compared to the unmodified PDMS case (*cf.* Fig. 6) due to a lower contact area between the particle and the substrate. We attribute this to an increase in surface modulus of the PDMS:UVO/PAA substrate relative to the unmodified PDMS support due to the UVO treatment step in the chemical modification process. In Fig. 8b, the addition of the LG layer increases the surface modulus compared to PDMS. In this case, the approach and retraction curves show a relatively large separation between the curves as the tip retracts from the surface. Fig. 8c depicts the interactions between the polymer coatings on the substrate and the particle. When the probe is in contact with the surface, the polymer chains on both the substrate and the particle are interacting *via* hydrogen bonding or electrostatic interactions, resulting in increased interactions between the two surfaces. As the probe begins to retract from the surface, the interactions between the surfaces remain in place up to a certain point, at which the polymer chains on the two surfaces disengage, and the interactions cease.

We evaluate the area between the approach and retractions curves for the three samples shown in Fig. 6–8 and report it in Fig. 9 as the work (W) done to separate the particle from the substrate. Fig. 9a displays the change in the work of separation between PDMS substrates and SiO_x particles as a function of chemical modification, which has been described in the experimental section. The data indicate that W depends on both the chemical nature of the substrate and the contact area between the particle and the substrate. W for the PDMS/SiO_x system is the highest among all cases studied primarily because of a large contact area between the substrate and the probing particle. We attribute the decrease in W after treating the PDMS with UVO to hardening the substrate and thus decreasing the number of interactions between the substrate and the particle. Surprisingly, PDMS:UVO substrates coated with PEI/PAA exhibit higher adhesion when interacting with bare SiO_x particles relative to the SiO_x particles coated with the PEI overcoat. While the values are within experimental error, we expected to detect the opposite behavior. One possible source of error is the large scatter in adhesion data (see Fig. S12 in the ESI†). We attribute this to inhomogeneities in the PEI/PAA layer on the PDMS:UVO substrate. The quality of the film in layer-by-layer (LbL) deposition depends on the interaction strength between the substrate and the first deposited layer.[45] Often multiple bilayers need to be deposited before a well-defined film is formed. We only used one bilayer in our work. We speculate that the PEI film did not attach strongly and uniformly to the PDMS:UVO substrate giving rise to an inhomogeneous PEI primer, which, in turn, influenced the poor quality of the PAA overcoat layer (see Fig. S12 in the ESI†).

Depositing LG on top of the PDMS substrate hardens the substrate and decreases the area of contact between the substrate and the particle. This leads to a substantial decrease in W relative to the PDMS/SiO_x particle case. Fig. 9b plots W between LG coated substrates and SiO_x particles as a function of particle chemical modification. The value of W for the interaction between the bare SiO_x particle and PDMS:UVO/PEI/LG and PDMS:UVO/PEI/LG/PEI/PAA is very similar. However, the adhesion strength between the PDMS:UVO/PEI/LG/PEI/PAA substrate and the PEI-coated SiO_x particle is high. We attribute this result to strong adhesion between the PAA surface layer and the PEI coating on the SiO_x particle. The AFM maps presented in Fig. S13 (in ESI†) support this notion. In this case, the adhesion between the particle and the substrate is dictated primarily by the strength of the interaction rather than the number of contacts. Additionally, we observe that the adhesion strength in the PDMS:UVO surface-functionalized with PAA is lower than that of the LG counterpart when probed by the PEI-functionalized SiO_x particle but within experimental error. We speculate that this could be due to inhomogeneities in the chemical functionalization of the substrate as described

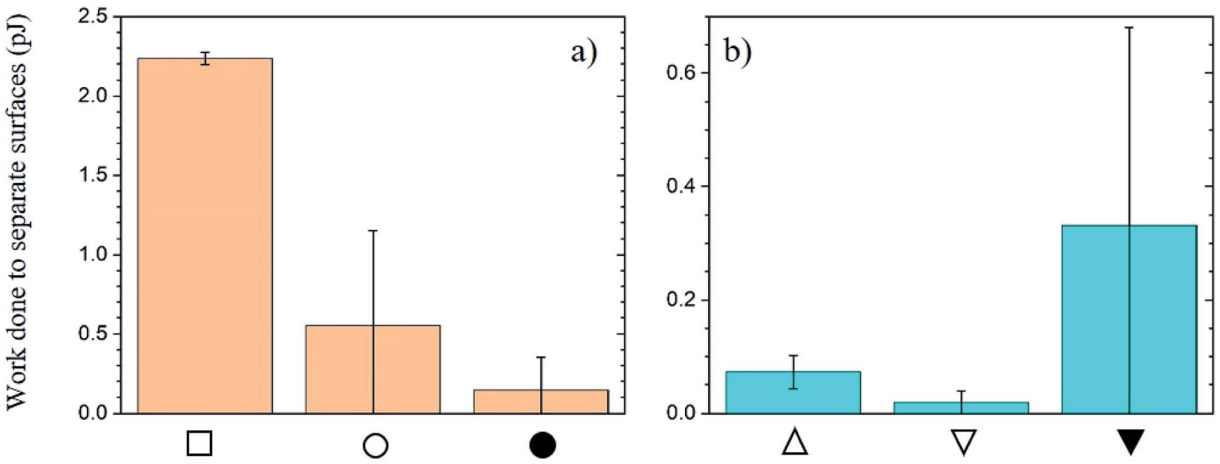

Fig. 9 Calculated work done to separate the substrates and particle as a function of chemical modification and surface modification. (a) PDMS substrate probed by SiO_x particle; (b) PDMS substrate coated with LG probed by SiO_x particle. Experimental conditions represented by the symbols are as follows: PDMS–SiO_x (□), PDMS:UVO/PAA–SiO_x (○), PDMS:UVO/PAA–SiO_x/PEI (●), PDMS:UVO/PEI/LG-SiO_x (△), PDMS:UVO/PEI/LG/PAA–SiO_x (▽), PDMS:UVO/PEI/LG/PAA–SiO_x/PEI (▼). Error bars represent the standard deviations.

previously, or instability of chemical functionalization of the particle. It is possible that the surface chemical coating degrades throughout repeated AFM scans. Consequently, interactions between the probe and substrate could be reduced.

Conclusion

In this work, we considered the interactions between SiO_x particles and substrates, in which we varied systematically the topographical feature geometry, the chemical composition of the coating, and substrate modulus. We studied the effect of these surface attributes on the interactions between the substrate and the probing particle using optical and laser scanning microscopy, and colloidal probe microscopy. We fabricated PDMS substrates with a variable aspect ratio ($AR = A/\lambda$) and studied the settlement of SiO_x beads onto such substrate from aqueous solutions. We further functionalized the surface of the PDMS substrate with PEI and PAA, and the surface of the particle with PEI to comprehend the impact of inter-surface interactions on settlement patterns. We also modified the PDMS surface with liquid glass (which was further functionalized using PEI and PAA) to understand how surface modulus impacts particle settlement. Higher AR features encouraged settlement of particles along the sides of the channel compared with substrates with lower aspect ratio. However, we only observed this effect in compliant PDMS substrates. This suggests that substrate modulus played a role in whether the particles were confined to the channels or are dispersed along the sides of the channels. We quantified interactions between the surface and particle as a function of surface modulus and chemical modification using a spherically modified AFM tip. These data showed that when the substrate modulus was low (*i.e.*, PDMS), the particle settlement was affected by the contact area between the particle and the substrate. Upon increasing the substrate modulus, the particle settlement on the substrate is governed only by the interactions between the substrate and the particle and not the deformation of the PDMS channel. The results suggest that particle settlement on the substrate involves a complex interplay between the particle size and chemistry and the surface chemistry, geometry, and surface modulus of the substrate.

Conflicts of interest

There are no conflicts to declare.

Acknowledgements

This work was supported by the C. Frank and Doris Culberson funding at NC State University. This work was performed in part at the Analytical Instrumentation Facility (AIF) at North Carolina State University, which is supported by the State of North Carolina and the National Science Foundation (award number ECCS-1542015). The AIF is a member of the North Carolina Research Triangle Nanotechnology Network (RTNN), a site in the National Nanotechnology Coordinated Infrastructure (NNCI).

References

1 A. Solga, Z. Cerman, B. F. Striffler and M. Spaeth, The Dream of Staying Clean: Lotus and Biomimetic Surfaces, *Bioinspiration Biomimetics*, 2007, **2**, S126–S134.
2 S. Ma, Q. Ye, X. Pei, D. Wang and F. Zhou, Antifouling on Gecko's Feet Inspired Fibrillar Surfaces: Evolving from Land to Marine and from Liquid Repellency to Algae Resistance, *Adv. Mater. Interfaces*, 2015, **2**(13), 1–12.
3 B. Bhushan and R. A. Sayer, Surface Characterization and Friction of a Bio-Inspired Reversible Adhesive Tape, *Microsyst. Technol.*, 2007, **13**, 71–78.
4 T. Sun and L. Feng, Bioinspired Surfaces with Special Wettability, *Acc. Chem. Res.*, 2005, **38**, 644–652.
5 Y. Zhang, S. E. Chen, J. Shao and J. J. van den Beucken, Combinatorial Surface Roughness Effects on Osteoclastogenesis and Osteogenesis, *ACS Appl. Mater. Interfaces*, 2018, **10**, 36652–36663.
6 S. Nishimoto and B. Bhushan, Bioinspired Self-Cleaning Surfaces with Superhydrophobicity, Superoleophobicity, and Superhydrophilicity, *RSC Adv.*, 2013, **3**, 671–690.
7 A. G. Sciancalepore, M. Moffa, D. Iandolo, G. S. Netti, C. Prattichizzo, G. Grandaliano, G. Lucarelli, L. Cormio, L. Gesualdo and D. Pisignano, Aligned Nanofiber Topographies Enhance the Differentiation of Adult Renal Stem Cells into Glomerular Podocytes, *Adv. Eng. Mater.*, 2018, **20**, 1–10.
8 L. Pocivavsek, J. Pugar, R. O'Dea, S. H. Ye, W. Wagner, E. Tzeng, S. Velankar and E. Cerda, Topography-Driven Surface Renewal, *Nat. Phys.*, 2018, **14**(9), 948–953.
9 P. R. Pitrez, L. Estronca, H. Vazão, A. L. Egesipe, A. Le Corf, C. Navarro, N. Lévy, A. De Sandre-Giovannoli, X. Nissan and L. Ferreira, Substrate Topography Modulates Cell Aging on a Progeria Cell Model, *ACS Biomater. Sci. Eng.*, 2018, **4**(5), 1498–1504.
10 T. Wu, H. Suzuki, Y. Su, Z. Tang, L. Zhang and T. Yomo, Bio-Inspired 3D Self-Patterning of Functional Coatings for PDMS Microfluidics, *Soft Matter*, 2013, **9**, 2311–2314.
11 Z. Pan, F. Cheng and B. Zhao, Bio-Inspired Polymeric Structures with Special Wettability and Their Applications: An Overview, *Polymers*, 2017, **9**, 1–33.
12 C. M. Grozea and G. C. Walker, Approaches in Designing Non-Toxic Polymer Surfaces to Deter Marine Biofouling, *Soft Matter*, 2009, **5**, 4088–4100.
13 D. G. Bock, M. E. Cristescu and C. W. Mckindsey, Effect of Shipping Traffic on Biofouling Invasion Success at Population and Community Levels, *Biol. Invasions*, 2016, **18**, 3681–3695.
14 S. Kitamura, M. Akizuki, J. Song and K. Nakayama, Tributyltin Exposure Increases Mortality of Nodavirus Infected Japanese Medaka Oryzias Latipes Larvae, *Mar. Pollut. Bull.*, 2017, **124**, 835–838.
15 M. Lejars, A. Margaillan and C. Bressy, Fouling Release Coatings: A Nontoxic Alternative to Biocidal Antifouling Coatings, *Chem. Rev.*, 2012, **112**(8), 4347–4390.

16 K. Liu and L. Jiang, Bio-Inspired Design of Multiscale Structures for Function Integration, *Nano Today*, 2011, **6**(2), 155–175.
17 G. D. Bixler and B. Bhushan, Review Article: Biofouling: Lessons from Nature, *Philos. Trans. R. Soc., A*, 2012, **370**(1967), 2381–2417.
18 J. Guenther, G. Walker-Smith, A. Warén and R. De Nys, Fouling-Resistant Surfaces of Tropical Sea Stars, *Biofouling*, 2007, **23**(6), 413–418.
19 M. Zhang, S. Feng, L. Wang and Y. Zheng, Lotus Effect in Wetting and Self-Cleaning, *Biotribology*, 2016, **5**, 31–43.
20 V. Barreau, R. Hensel, N. K. Guimard, A. Ghatak, R. M. McMeeking and E. Arzt, Fibrillar Elastomeric Micropatterns Create Tunable Adhesion Even to Rough Surfaces, *Adv. Funct. Mater.*, 2016, **26**(26), 4687–4694.
21 A. M. Brzozowska, S. J. Maassen, R. Goh Zhi Rong, P. I. Benke, C.-S. Lim, E. M. Marzinelli, D. Jańczewski, S. L.-M. Teo and G. J. Vancso, Effect of Variations in Micro-Patterns and Surface Modulus on Marine Fouling of Engineering Polymers, *ACS Appl. Mater. Interfaces*, 2017, **9**, 17508–17516.
22 S. Wu, F. Zuber, K. Maniura-Weber, J. Brugger and Q. Ren, Nanostructured Surface Topographies Have an Effect on Bactericidal Activity, *J. Nanobiotechnol.*, 2018, **16**, 1–9.
23 Y. C. Chen, Z. S. Huang and H. Yang, Cicada-Wing-Inspired Self-Cleaning Antireflection Coatings on Polymer Substrates, *ACS Appl. Mater. Interfaces*, 2015, **7**(45), 25495–25505.
24 A. V. Bers, E. R. Diaz, B. A. P. da Gama, F. Vieira-Silva, S. Dobretsov, N. Valdivia, M. Thiel, A. J. Scardino, C. D. McQuaid, H. E. Sudgen, *et al.*, Relevance of Mytilid Shell Microtopographies for Fouling Defence - a Global Comparison, *Biofouling*, 2010, **26**(3), 367–377.
25 S. Chang, X. Chen, S. Jiang, J. Chen and L. Shi, Using Micro-Patterned Surfaces to Inhibit Settlement and Biofilm Formation by Bacillus Subtilis, *Can. J. Microbiol.*, 2017, **63**(7), 608–620.
26 W. Choi, C. Lee, Y. J. Won, D. Lee, G. W. Lee, M. G. Shin, B. Chun, T.-S. Kim, H.-D. Park, H. W. Jung, *et al.*, Sharkskin-Mimetic Desalination Membranes with Ultralow Biofouling, *J. Mater. Chem. A*, 2018, **6**, 23034–23045.
27 C. M. Magin, S. P. Cooper and A. B. Brennan, Non-Toxic Antifouling Strategies, *Mater. Today*, 2010, **13**(4), 36–44.
28 F. W. Y. Myan, J. Walker and O. Paramor, The Interaction of Marine Fouling Organisms with Topography of Varied Scale and Geometry: A Review, *Biointerphases*, 2013, **8**, 1–13.
29 E. Ralston and G. Swain, Bioinspiration–The Solution for Biofouling Control?, *Bioinspiration Biomimetics*, 2009, **4**, 1–9.
30 A. V. Bers and M. Wahl, The Influence of Natural Surface Microtopographies on Fouling, *Biofouling*, 2004, **20**(1), 43–51.
31 J. Genzer and A. Marmur, Biological and Synthetic Self-Cleaning Surfaces, *MRS Bull.*, 2008, **33**, 742–746.
32 B. Dean and B. Bhushan, Shark-Skin Surfaces for Fluid-Drag Reduction in Turbulent Flow: A Review, *Philos. Trans. R. Soc., A*, 2010, **368**, 4775–4806.
33 S. Erramilli and J. Genzer, *Soft Matter*, 2019, **15**, 4045–4067, DOI: 10.1039/c9sm00527g.
34 A. J. Scardino, J. Guenther and R. de Nys, Attachment Point Theory Revisited: The Fouling Response to a Microtextured Matrix, *Biofouling*, 2008, **24**(1), 45–53.
35 A. J. Scardino, E. Harvey and R. De Nys, Testing Attachment Point Theory: Diatom Attachment on Microtextured Polyimide Biomimics, *Biofouling*, 2006, **22**, 55–60.
36 J. Genzer and J. Groenewold, Soft Matter with Hard Skin: From Skin Wrinkles to Templating and Material Characterization, *Soft*, 2006, **2**, 310–323.
37 K. Efimenko, M. Rackaitis, E. Manias, A. Vaziri, L. Mahadevan and J. Genzer, Nested Self-Similar Wrinkling Patterns in Skins, *Nat. Mater.*, 2005, **4**, 293–297.
38 C. Lu, H. Mohwald and A. Fery, A Lithography-Free Method for Directed Colloidal Crystal Assembly Based on Wrinkling, *Soft Matter*, 2007, **3**, 1530–1536.
39 Y. Yu, C. Ng, T. A. F. Konig and A. Fery, Tackling the Scalability Challenge in Plasmonics by Wrinkle-Assisted Colloidal Self-Assembly, *Langmuir*, 2019, **35**, 8629–8645.
40 P. K. Schoch and J. Genzer, Adsorption of Multiple Spherical Particles onto Sinusoidally Corrugated Substrates, *Langmuir*, 2014, **30**, 9407–9427.
41 P. K. Schoch and J. Genzer, Adsorption of "Soft" Spherical Particles onto Sinusoidally-Corrugated Substrates, *Soft Matter*, 2014, **10**, 7452–7458.
42 P. K. Schoch and J. Genzer, Adsorption of Size-Polydisperse Particles on Sinusoidally Corrugated Surfaces, *Mol. Simul.*, 2018, **44**(6), 494–506.
43 Y. Yang, M. Haile, Y. T. Park, F. A. Malek and J. C. Grunlan, Super Gas Barrier of All-Polymer Multilayer Thin Films, *Macromolecules*, 2011, **44**, 1450–1459.
44 R. Schmitz, *Investigating and Counteracting Phenomena That Govern Polymer Microsphere Fouling on Wind Tunnel Screens*, North Carolina State University, 2019.
45 P. T. Hammond, Form and Function in Multilayer Assembly: New Applications at the Nanoscale, *Adv. Mater.*, 2004, **16**(15), 1271–1293.

